
Proceedings Paper:
Miyashita, S., Guitron, S., Yoshida, K. et al. (3 more authors) (2016) Ingestible, controllable, and degradable origami robot for patching stomach wounds. In: Proceedings - IEEE International Conference on Robotics and Automation. 2016 IEEE International Conference on Robotics and Automation (ICRA),, 16-21 May 2016, Stockholm, Sweden. , pp. 909-916. ISBN 9781467380263

https://doi.org/10.1109/ICRA.2016.7487222

Ingestible, Controllable, and Degradable Origami Robot for Patching Stomach Wounds

Shuhei Miyashita[1], Steven Guitron[1], Kazuhiro Yoshida[2], Shuguang Li[1], Dana D. Damian[3], and Daniela Rus[1]

***Abstract*— Developing miniature robots that can carry out versatile clinical procedures inside the body under the remote instructions of medical professionals has been a long time challenge. In this paper, we present origami-based robots that can be ingested into the stomach, locomote to a desired location, patch a wound, remove a foreign body, deliver drugs, and biodegrade. We designed and fabricated composite material sheets for a biocompatible and biodegradable robot that can be encapsulated in ice for delivery through the esophagus, embed a drug layer that is passively released to a wounded area, and be remotely controlled to carry out underwater maneuvers specific to the tasks using magnetic fields. The performances of the robots are demonstrated in a simulated physical environment consisting of an esophagus and stomach with properties similar to the biological organs.**

I. Introduction

Miniature origami robots can provide versatile capabilities for gastrointestinal interventions, especially when used in conjunction with imaging technologies, as they can move and manipulate with a high degree of control and be minimally invasive for the patient. Our previous work [1] has demonstrated a mobile origami robot that self-folds, is remotely controllable, and can be dissolved to be recycled. In this paper we design and control a new origami robot that can be swallowed and sent through the esophagus to the stomach (Fig. 1). Once in the stomach, the robot self-deploys and is controllable using an external magnetic field to reach a location of interest where it can use its body to patch a wound such as an inflammation made by an accidentally swallowed battery. Origami robot designs are well suited for tasks that require multiple modalities of locomotion, such as traveling through the esophagus and the stomach, because they can do the first task in a compact shape (e.g. a pill shape) and then morph to enable a solution for the second task. Additionally, building on our work described in [1] we can manipulate the trajectory of the robot using an external magnetic field. We believe that these techniques for creating origami robots provide a non-invasive method for clinical interventions.

One example of clinical interventions where a multifunction miniature robot is desired is the ingestion of button batteries. It is reported that more than 3500 people of all ages ingest button batteries in the United States every year, and the incidence is growing (National Capital Poison Center; [2]). 46 deaths and 183 cases with severe esophageal or airway burns and subsequent complications have been reported in the last 40 years. Most of the victims are children. Having considered the fatality of these accidents and the availability of efficient interventional tools to counteract them, this study approached the problem by deploying a miniature biodegradable origami robot in the stomach, guided to a wounded location, where it had the ability to remove a lodged battery, patch and effectively administer drugs directly to the wounded location, and eventually dispose itself on-site by biodegradation or digestion.

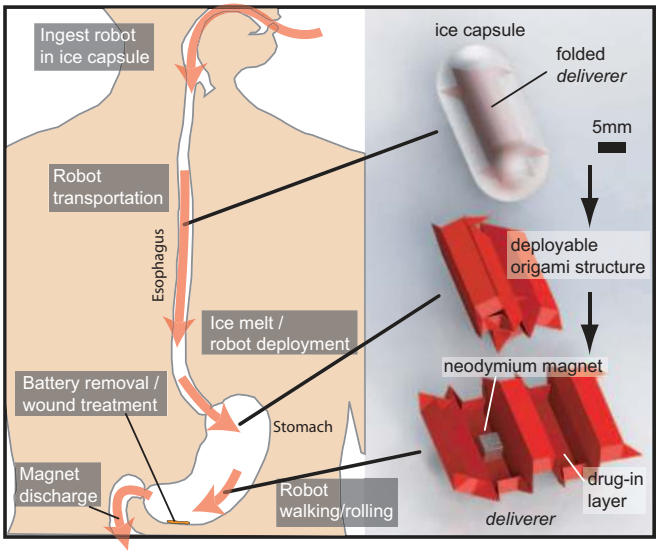

Fig. 1. The developed system. An iced robot is transported into an artificial stomach. Once the ice melts and the robot is deployed, the robot is controlled using a remote magnetic field. The robot removes a foreign body, such as a button battery, from the location and further treats an inflammation by delivering a drug.

There are several design, fabrication, modeling and control challenges we address in this work: (1) Miniature robot body design, bypassing the integration of conventional electronics; (2) Method for intact, instant, and compact transportation to an affected area and minimum invasiveness of the robot (3) Soft and 2D material selection, deployment and (mechanically) functional robot design; (4) Method for non-invasive remote control signal transmission and remote actuation; (5) After-operation in-situ removal or biodegradable material selection. This paper contributes (1) Material composition for a biodegradable and biocompatible robot; (2) Concept of ice-encapsulated robot for safe transportation into the stomach;

Support for this work has been provided by NSF grants 1240383 and 1138967. [1]Computer Science and Artificial Intelligence Laboratory, MIT. 32 Vassar street, Cambridge, MA, 02139, USA. shuheim@csail.mit.edu [2]Department of Mechano-Micro Engineering, Tokyo Institute of Technology. [3]Department of Automatic Control and System Engineering, Centre of Assistive Technology and Connected Healthcare, University of Sheffield. Shuhei Miyashita is currently with the Department of Electronics, University of York, UK.

(3) Deployable origami design for wide range affected area coverage, developed fit-in-capsule origami robot design and fabrication, integrating a drug delivery layer; (4) Remote magnetic control for rolling and underwater walking; (5) Physics modeling and analysis of the robots dynamics; (6) Pilot tests with an artificial stomach and esophagus created using a new silicone molding process.

II. Related work

There is considerable progress in interventional technologies for the gastrointestinal tract. For example, capsule endoscopy is one of the representative advancements in this field focused on embedding vision into engineered capsules that can be transported through the gastrointestinal tract for diagnosis, thus replacing current tethered endoscopes [3], [4], [5], [6], [7], [8], [9]. These technologies can visualize a large part of the gastrointestinal lining. Some current technologies targeted for use inside the body include ophthalmologic robots [10], esophageal robotic implants [11], and origami stents [13]. Large efforts are still directed toward microsurgical tools that are minimally invasive, biocompatible, multifunctional, and well accepted by patients [14], [15], [16]. Due to difficulty with current treatment procedures, there is a need for miniature surgical robots that, aside from diagnosis, can potentially perform multiple medical or surgical tasks *in vivo* such as non-invasive transportation and deployment in a targeted location, mechanical operations on tissues or fluids, such as delivery, insertion and inflation [12], microanchoring [17] or gripping [18], removal, patching, piercing, sampling, and biodegradation. Origami robots promise to provide solutions to most of these tasks with minimal on-board electronics.

III. Stomach simulator

In this study, we have developed a physical environment for testing the performance of our robotic system, comprised of an artificial esophagus and a silicone stomach that feature a biologically-comparable stiffness and folded lining inside (Fig. 2). The artificial organs (1) provide a nonperishable, realistic, cost-effective environment for iterative tests of the structure and function of the robot, and (2) allow easy parameterization of the artificial environment, such as the size of the organs and location of the damaged area. This section shows the recipe to produce such an environment, which we could not find in the literature.

A. Artificial stomach fabrication

The stomach is a muscular and hollow organ of the digestive system, responsible for breaking down food. Fig. 2 (top) shows an overview of the artificial stomach and a magnification of lining folds (bottom). Following the size specifications of an average human stomach, the stomach has a maximum width of 10 cm. We reproduced the stomach environment using a template silicone mold technique to be mechanically analogous to the real tissues. In this study, we put emphasis on the mechanical attributes of the stomach such as structure, stiffness, friction, fluid viscosity, and color,

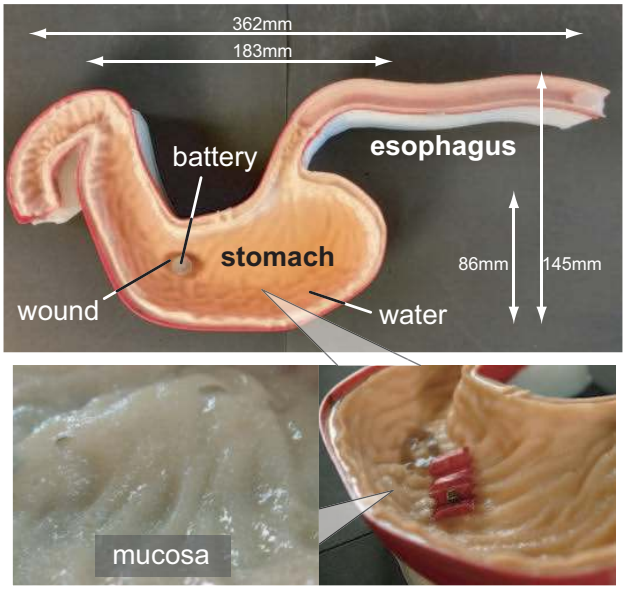

Fig. 2. Developed artificial esophagus and stomach (top) and details of the artificial mucosa (bottom).

while omitting other properties such as temperature, pH, peristaltic motion of the esophagus, or volumetric dynamics of the stomach.

To define the design guidelines necessary to simulate the real environment, we experimentally investigated the stiffness of pig stomach samples. We measured compressive and tensile stresses of rectangular pig stomach samples ($15 \times 30 \times 5\,\text{mm}^3$, length×width×height) using an Instron Machine (Instron 5944). For compressive stress, a rectangular iron bar with a contact area of $11 \times 14\,\text{mm}^2$ was used to apply pressure to the tissue, and for tensile stress, grippers with a rough surface (built using rapid prototyping) of size $40 \times 30\,\text{mm}^2$ were used to grip the slippery tissues when stretched (Fig. 3 (a),(b), respectively). The pig's stomach was fresh (within 24 hours from collection) and preserved at $-4°\text{C}$ before being used.

Fig. 3 (c)(d) shows the plots characterizing the stiffness properties of the biological and artificial stomach tissues, depending on the mechanical deformation applied, i.e., compressive and tensile stress. We computed the average fitted lines for the biological stomach profiles, resulting in the equations $S\,[kgf] = 0.72\,C\,[mm] - 1.06$ and $S\,[kgf] = 0.04\,E\,[mm] - 0.19$ for compression and extension, respectively. In the case of the biological stomach, we only considered the initial tissue deformation depicted by the first increasing curve, given the limited tissue deformation capabilities expected from our robot. These values were most closely matched with Ecoflex molding silicone whose average fitted lines were $S\,[kgf] = 1.03\,C\,[mm] + 0.68$ and $S\,[kgf] = 0.01\,E\,[mm] + 0.07$ for compression and extension, respectively. These equations show that a reasonable match between the stiffness of the biological and artificial stomach samples was achieved.

The mold templates of the esophagus and stomach were

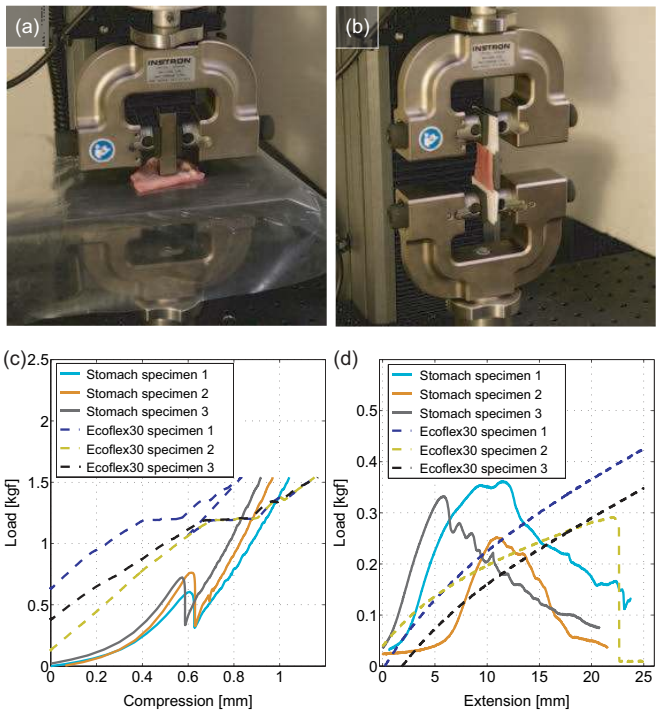

Fig. 3. Tissue testing and stiffness characteristics. (a-b) Experimental outlook with Instron Machine; compressive stress measurement (in a), and extension measurement (in b). (c) Stiffness of biological pig stomach tissue and Ecoflex 00-30 samples during compressive tests, (d) Stiffness of biological pig stomach tissue and Ecoflex 00-30 samples during tensile tests.

3D printed (Fortus by Stratasys, 250 mc and 400 mc) using a market available CAD model (Turbosquid). We first 3D printed molds of the outer and inner parts of the stomach and esophagus. The inside mold was used to create a reverse mold of the lining. We used this latter mold and the outside part to compose the final product. Mold Star 15 Slow (Smooth-On) was used to fabricate the reverse mold. The final product is made of Ecoflex 00-30 (Smooth-On) to match the stiffness of the pig's stomach, and colored with Silc Pig colors Flesh PMS 488C and Yellow PMS 107C (2 Flesh : 1 Yellow). The stomach wall has a thickness ranging between 3.5 and 5.5 mm due to the ridges of mucosa.

In general, the stomach is filled with gastric fluid and the walls of both the esophagus and the stomach are lubricated with mucosa secretion and body fluids. Though the viscosity of gastric fluid can be variable, when the stomach is filled with water, its viscosity can be approximated as 1 centistoke. For the investigation of the biodegradability of the developed robot, we used market available Simulated Gastric Fluid (Fisher Scientific) which contains 0.2% sodium chloride in 0.7% hydrochloric acid solution (pH: $1.0 \sim 1.4$).

B. Ulcer formation

This experiment assesses the prospective damage of the stomach wall caused by a button battery that was accidentally ingested. In order to reproduce realistic inflammation of the tissue, we generated a damaged area of an *ex vivo* tissue using a button battery. We gently sandwiched a button battery (303 battery, 175 mAh) and tissue (ham slice, 2.3 mm thickness) using two acrylic plates for 60 minutes.

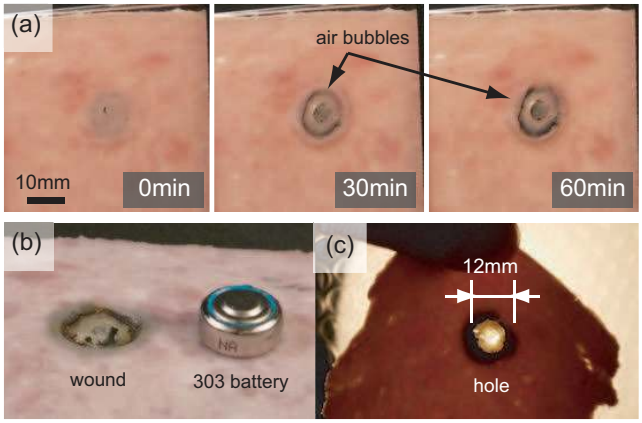

Fig. 4. Damage on a meat wall caused by a button battery. (a) Time lapse images, (b) battery and the created wound, and (c) the hole.

Fig. 4 (a) shows the time lapse of tissue wall damage, taken from the opposite side of where the battery was placed. After a few minutes, air bubbles were observed at the interface between the battery and the tissue due to an electric current flow. In 30 minutes, degradation of the tissue was observed from the opposite side of the tissue. In 60 minutes, a hole of 12 mm diameter was created (Fig. 4 (b),(c)), clearly displaying the danger of accidental ingestion.

IV. Robot Design and Remote Control

We developed two types of origami robots, which we will further refer to as the battery *remover* and the drug *deliverer*, respectively, for the treatment of stomach inflammation. The origami designs were chosen to fold the robot such that they can be embedded in ice capsules which can be swallowed, carried to the stomach and dissolved. The robots are controlled by an electromagnetic actuation system developed in our group [1]. The actuation system consists of 4 cylindrical coils, inclined 45°, distanced 25 cm each center to center, surrounding the center of the work stage, and placed at the lower hemisphere. By running currents, a magnetic field of various strengths and directions can be generated on the work stage. We visually observe the position of the robot. In real clinical applications we plan to employ a combination of ultrasound, X-ray, and an array of hall effect sensors to localize the position of the battery and the robot.

The following sections explain the robot's architecture (Section IV-A), encapsulation (IV-B), material (Section IV-C), and control (Sections IV-D and Section IV-E).

A. Robot architecture

In the first phase, the *remover* removes a battery from the inflammation spot to prevent further damage of the stomach wall while the robot is in a capsule shape. The *remover*, featuring a minimum supporting structure, is folded in an elliptic cylinder package ($\Phi_1 = 3$ mm, $\Phi_2 = 1$ cm, 1 cm long) and frozen. The shape allows rotational motion even

after the encapsulating ice melts. The structure contains a diametrically oriented cubic neodymium magnet (edge length $a = 3.2\,\text{mm}$) attached at the center of the robot's structure. The *remover* is fixed in an ice capsule for easy swallowing and digestion, expected for the short-lasting stay in the stomach. After the patient swallows the ice capsule using water, the *remover* travels by rolling in the stomach, actuated by controlled magnetic fields and guided to the location of the battery. It then grabs the battery by magnetic attraction, and dislocates it from the inflammation site. The magnet-battery distance changes over time due to ice melting, altering the magnitude and direction of torque transmitted to the battery, thus enabling diverse lift postures. In order to induce maximum torque for lifting the battery, the magnet should be oriented planar to the battery (instead of perpendicular to it). The ice dissolution approach enhances the probability of a proper attachment, as the magnet steadily reorients itself while the ice melts to maximize the connection strength. Magnet reorientation while melting also reduces the risk of the magnet and battery magnetically pinching the mucosa.

After the battery and *remover* are removed from the body through the gastrointestinal tract, in a subsequent phase, the *deliverer* is sent to the stomach (Fig. 5). The role of the *deliverer* is to walk in the stomach and patch the inflammation site by landing on it, releasing a drug to the damaged area through the robot's body degradation. In order to effectively administer the drug, the *deliverer* should have a wide surface area covering the inflammation when deployed from the ice capsule. An origami technique is used to design the body as an accordion shape. This body structure enables the robot to compactly fold inside the ice capsule and expand 5 times when deployed.

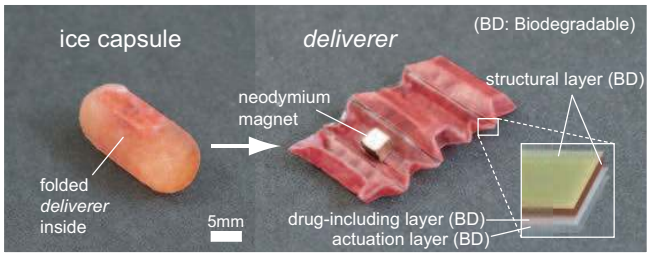

Fig. 5. Ice capsule and *deliverer*. Ice capsule is colored with food coloring for video recording purpose.

The *deliverer* consists of 5 trapezoidal boxed segments which can be stacked and configured as a hexagonal cylinder by folding. The front and back of the robot are designed to be point symmetric such that it induces asymmetric friction force along the body axis (see Section IV-E). The robot can locomote even when flipped. A cubic neodymium magnet is contained in the second segment. The magnet is oriented along the longitudinal axis of the body to induce an asymmetric moment of inertia under a periodic magnetic field application. The magnet is concealed when the body forms a hexagonal cylinder in an ice capsule.

The *deliverer* was pre-folded using the technique in [19] with a hot plate. When the layered flat body was exposed to heat of $100°\text{C}$, the Biolefin layer shrunk causing the entire structure to fold itself into the final configuration without human intervention. While the materials composing the body are biodegradable (see Section IV-C), the entire body keeps its shape despite the temperature and even in ice. After drug delivery and robot degradation, the magnet can be removed naturally through the gastrointestinal tract.

B. Ice capsule transportation

Ice capsule transportation has various advantages over other approaches such as encapsulation by gelatin or sugar. First, it is safe and reduces friction while sliding through the esophagus by peristalsis. Second, it disappears quickly and completely *in vivo* by melting once it reaches the stomach, and thus it doesn't hinder the robot's motions unlike other materials, which we realized to be critical. Third, it is easily produced.

The ice capsule is $27.0\,\text{mm}$ long, almost the same size as the 000 standard pill size (length$= 26.14\,\text{mm}$, diameter$= 9.97\,\text{mm}$), and it melts in water on the order of a minute to a few minutes depending on the temperature. The size is determined such that the capsule (mass $w = 2.55\,\text{g}$, volume $2.22\times10^{-6}\,\text{m}^3$) sinks in water considering the robot's weight ($w_r = 0.578\,\text{g}$), and is subject to scaling down for childrens' use. For freezing an ice capsule robot, we first 3D printed a capsule from ABS material. Then, we placed the capsule in a silicone mold, molded it, and retracted the capsule from the mold such that the mold retained a capsule-shaped hollow space inside. We finally put the robot in the hollow space, filled it with water, and froze it in a freezer.

C. Material selection

For *in vivo* use, the robot's body needs to be composed of biocompabitle and biodegradable materials. The *deliverer's* body is made of 5 different layers (Fig. 5); (1) polyolefin structural layer (biodegradable (BD)), (2) organic structural layer (pig intestine wall, Eastman outdoors, BD), (3) drug-including layer (simulated by oblate, PIP, water dissolvable), and (4) actuation layer for self-folding (heat sensitive shrinking film Biolefin, National Shrinkwrap, BD, deforms at $65°\text{C}$), adhered by (5) silicone adhesive layers (McMaster). Before the *deliverer* is self-folded, the layers are laminated symmetrically by the Biolefin layer (see [1]).

Choosing differing biodegradable layers allows for layer degradation at different time scales such that they fulfill their operational requirements at designed time sequences. The organic structural layer is expected to degrade at the slowest speed while the drug doping layer is expected to degrade constantly and release the ingredient. Although the adhesive we used is not medical grade, silicone is a biocompatible material. There are many medical grade, or edible adhesives off the shelf which will be used for a future model. Note that although all materials were selected for their biodegradability or biocompatibility, further investigations on the medical grade safety check are still required.

Fig. 6 shows the degradation process of the *deliverer's* body, partially placed in simulated gastric fluid set at body

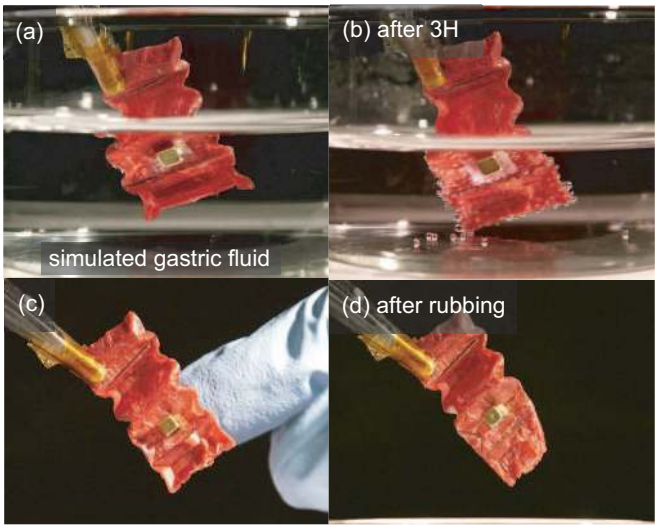

Fig. 6. *Deliverer*'s biodegradability. The *deliverer* is partially placed in simulated gastric fluid for 3 hours showing biodegradability.

temperature (37°C) for 3 hours. Although the process took a while, the remains of the *deliverer* (including the magnet) are expected to be expelled from the body. The entire process shows that the presence of the *deliverer* as a foreign body has low probability to harm the gastrointestinal tract. In real stomach, there exist enzymes such as pepsin, which should accelerate the degradation speed. For safety, no more than two magnets can be in the gastrointestinal tract at the same time.

D. In-capsule rolling motion control

The ice capsules and the *deliverer* are remotely actuated by an electromagnetic actuation system developed in our group [1]. We developed two control modes: a rolling mode for the ice capsules (Fig. 7 (a)), and a walking mode for the *deliverer* (Fig. 7 (b)). In rolling mode, an ice capsule is actuated by applying a rotating magnetic field. Fig. 7(a) shows the schematic of a magnet in a cylindrical structure (ice capsule) on a slope, carrying a load (303 battery). The slope has an angle θ, and the coordinate x is set along the slope. The structure has radius $R = 5.5\,\text{mm}$, length $L = 27\,\text{mm}$, an angle φ from the vertical plane, angular velocity ω, coefficient of friction μ_f and an applied friction force f_f, and mass $w = 2.55\,\text{g}$ where the equivalent mass in water is $w' = 0.33\,\text{g}$. The load has mass $w_L = 2.18\,\text{g}$ with equivalent mass $w'_L = 1.63\,\text{g}$ in water, and can be attached with either the longitudinal face of the battery whose magnet-battery distance L_L will become $L_L = 11.24\,\text{mm}$, or collateral face whose distance will be $L_L = 8.19\,\text{mm}$.

The neodymium magnet is cubic and has edge length $a = 3.2\,\text{mm}$, with dipole moment $m = 29.8 \times 10^{-3}\,\text{Am}^2$ in our experiment and $m = a^3 M_{sat} = 33.9 \times 10^{-3}\,\text{Am}^2$ in theory (we use $m = 29.8 \times 10^{-3}\,\text{Am}^2$ for calculations), where $M_{sat} = 1.03 \times 10^6\,\text{A/m}$ is the saturation magnetization of a neodymium magnet. The rotating magnetic flux density has absolute value of B, angle ψ from the vertical plane,

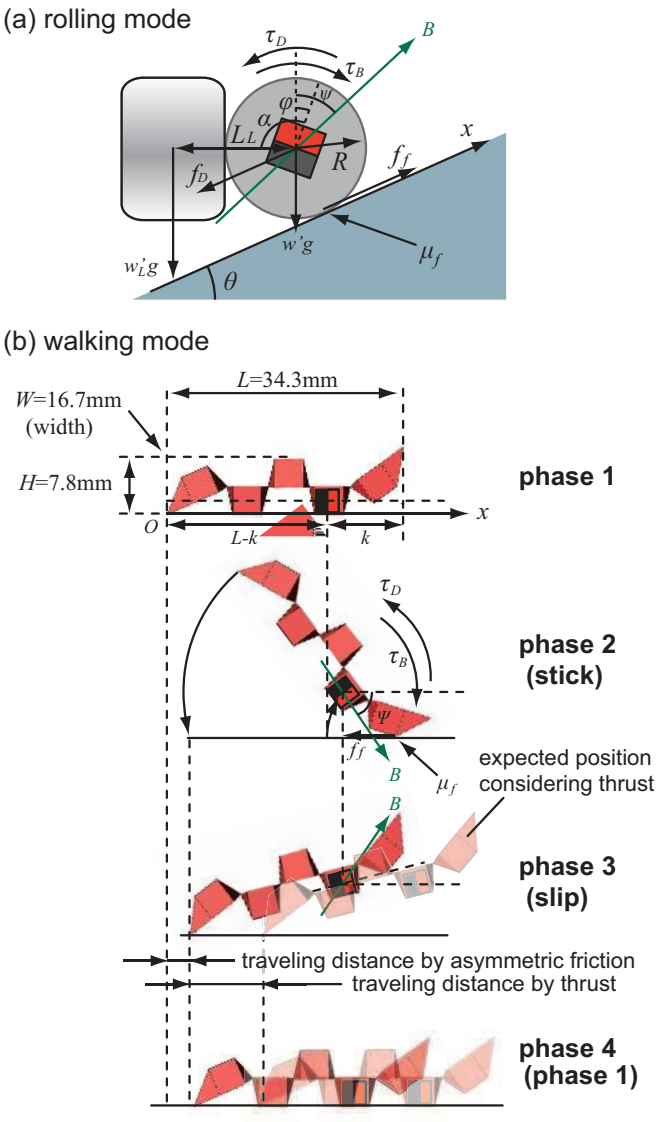

Fig. 7. Rolling mode for ice capsule (in a) and walking mode for *deliverer* (in b).

and it generates magnetic torque τ_B on the capsule. The fluidic drag force f_D and torque τ_D act on the capsule, and $g = 9.81\,\text{m/s}^2$. It is assumed that the density is homogeneous in the capsule.

Below we derive the governing equation for the ice capsule to climb the slope underwater and investigate the required B to lift a button battery.

The acting magnetic torque is

$$\tau_B = mB\sin(\psi - \varphi). \tag{1}$$

The equation of motion for translational motion is

$$w\frac{d^2x}{dt^2} + w_L\frac{d^2x_L}{dt^2} = f_f - (w' + w'_L)g\sin\theta - f_D, \tag{2}$$

where x_L is the x coordinate of the load.

The rotational motion is

$$(I + I_L)\frac{d^2\varphi}{dt^2} = \tau_B - f_f R - w'_L g L_L \sin(\alpha - \varphi) - \tau_D, \tag{3}$$

where $I = \frac{1}{2}wR^2$ is the moment of inertia of the capsule and I_L is that of the load around the center of the capsule.

Under no-slip condition $f_f < \mu_f(w' + w'_L)g\cos\theta$,

$$\frac{dx}{dt} = R\frac{d\varphi}{dt}, \tag{4}$$

and

$$x_L = x - L_L\cos\Big(\frac{\pi}{2} + \theta - (\alpha - \varphi)\Big). \tag{5}$$

Thus we obtain

$$\begin{aligned}\frac{d^2x_L}{dt^2} &= -L_L\omega^2\sin(\varphi - \alpha + \theta) \\ &\quad + \Big(R + L_L\cos(\varphi - \alpha + \theta)\Big)\frac{d^2\varphi}{dt^2}.\end{aligned} \tag{6}$$

Based on eqs. (2)–(6), we obtain the governing equation

$$\begin{aligned}&\Big[\Big\{\frac{3}{2}wR + \frac{I_L}{R} + w_L\big(R + L_L\cos(\varphi - \alpha + \theta)\big)\Big\}\frac{d^2\varphi}{dt^2} \\ &- w_LL_L\omega^2\sin(\varphi - \alpha + \theta) + (w' + w'_L)g\sin\theta + f_D\Big]R \\ &- w'_LgL_L\sin(\varphi - \alpha) + \tau_D = mB\sin(\psi - \varphi).\end{aligned} \tag{7}$$

With the controlled translational velocity $v = 32.2\,\text{mm/s}$ and angular velocity $\omega = 5.85\,\text{rad/s}$, the drag force f_D is

$$f_D \sim C_DRL\rho v^2, \tag{8}$$

where $C_D = 1.1$ is the drag coefficient obtained referring to [20] with derived Reynolds number 398 and the density of water at 25°C $\rho = 1000\,\text{kg/m}^3$. We obtain the drag force as $f_D = 1.69 \times 10^{-4}\,\text{N}$, which is negligibly small ($\frac{f_D}{\tau_B R} \ll 1$).

From the Navier-Stokes equation and the equation of continuity, the torque τ_D acting on the capsule is

$$\tau_D \sim 4\pi\mu_D RL\omega, \tag{9}$$

where $\mu_D = 0.89 \times 10^{-3}\,\text{Pa s}$ is the viscosity of the fluid (water, 25°C). We obtain $\tau_D = 9.71 \times 10^{-6}\,\text{Nm}$, which is, again, negligibly small ($\frac{\tau_D}{\tau_B} \ll 1$).

When the rotating magnetic field is applied slowly enough and the motion of the capsule is in steady state, namely when $\frac{L_L\omega^2}{g} \ll 1$ and $\frac{d^2\varphi}{dt^2} = 0$ hold, from eq. (7) we obtain the following condition for the required magnitude of B:

$$\sin(\psi - \varphi) = \frac{(w' + w'_L)gR\sin\theta - w'_LgL_L\sin(\varphi - \alpha)}{mB} \tag{10}$$

$$\begin{aligned}&(\leq 1) \\ \Rightarrow B \geq &\frac{(w' + w'_L)gR\sin\theta - w'_LgL_L\sin(\varphi - \alpha)}{m}\Big|_{\max} \\ = &\frac{\big((w' + w'_L)R\sin\theta + w'_LL_L\big)g}{m}.\end{aligned} \tag{11}$$

The most difficult situation is when the attachment occurs between the capsule and the side wall of the battery on a non-slope surface ($L_L = 11.24\,\text{mm}$, $\theta = 0$). It requires $B \sim 5\,\text{mT}$, which is relatively high. However, in a real case, there exist many options for carrying a battery, for example rotating the battery horizontally or rolling the capsule over the battery. Due to the strong attraction force of the magnet, we rarely observed slippage of the battery regardless of the low friction of the ice. When slippage between the ice capsule and the stomach surface occurs, the ice capsule exploits the uneven configuration with the carried battery for displacement.

E. Walking motion control for the Deliverer

The walking motion is designed based on stick-slip motion on ground [1]. The robot acts underwater and thus experiences effects from moving in a low Reynolds number environment. Fig. 7 (b) illustrates the walking motion of the *deliverer* seen from the side. The walking motion is easier to control than the rolling motion with higher precision.

The magnetic field is applied at 5 Hz in the direction along which the *deliverer* is actuated (the positive x direction in the figure) oscillating through four angles (Ψ, $\Psi/2$, $-\Psi/2$ and $-\Psi$; $\Psi = 1.1\,\text{rad}$ is the angle from the horizontal plane). When such an alternating field is applied, the *deliverer* can "walk forward" due to the combination of thrust, asymmetric frictional force induced by the shape between front and rear, and asymmetric mass balance of the body. More precisely, one step motion consists of three distinctive phases; (phase 1) the body is laid on the ground; (phase 2) the body points down following a downward-oriented magnetic field; (phase 3) the body points up following an upward-oriented magnetic field. From phase 1 to phase 2, the *deliverer* lifts up the rear while the front is still in contact keeping the anchor position against thrust and exploiting the friction (stick motion). The center of mass, assumed to be at the location of the magnet, travels forward a distance $\sim k(1-\cos\Psi)$, where $k = 8.7\,\text{mm}$ is the distance between the center of the magnet and the front edge. From phase 2 to phase 3, as a turn of magnetic field occurs instantly, and due to the relatively low Reynolds environment with negligibly light body mass compared to the magnet mass, the body is expected to rotate about the magnet keeping the height of the center of mass (slip motion). Due to the body balance shifted to the front and also depending on the frequency of B, the posture does not completely catch up to the magnetic field, compared to the posture in phase 2. Considering the thrust that acts to push the body backward, this angle of magnetic field pointing up is minimized. However if we set Ψ very small, for example ~ 0, the chance that the *deliverer* stumbles on mucosa increases. From phase 3 to phase 4 (which is the same state as phase 1), the *deliverer* exploits friction and low stroke, and enables further body travel.

The body length is $L = 34.3\,\text{mm}$, the height $H = 7.8\,\text{mm}$, and the width $W = 16.7\,\text{mm}$. The traveling distance D in one cycle without considering thrust is kinematically derived and is

$$D \approx L - k\cos\Psi - (L-k)\cos\Big(\sin^{-1}\big(\frac{k\sin\Psi}{L-k}\big)\Big). \tag{12}$$

With this function, the walking speed of the *deliverer* is estimated to be 2.98 cm/s. Our experimental result shows the walking speed to be 3.71 cm/s. The difference is due to the influence of thrust.

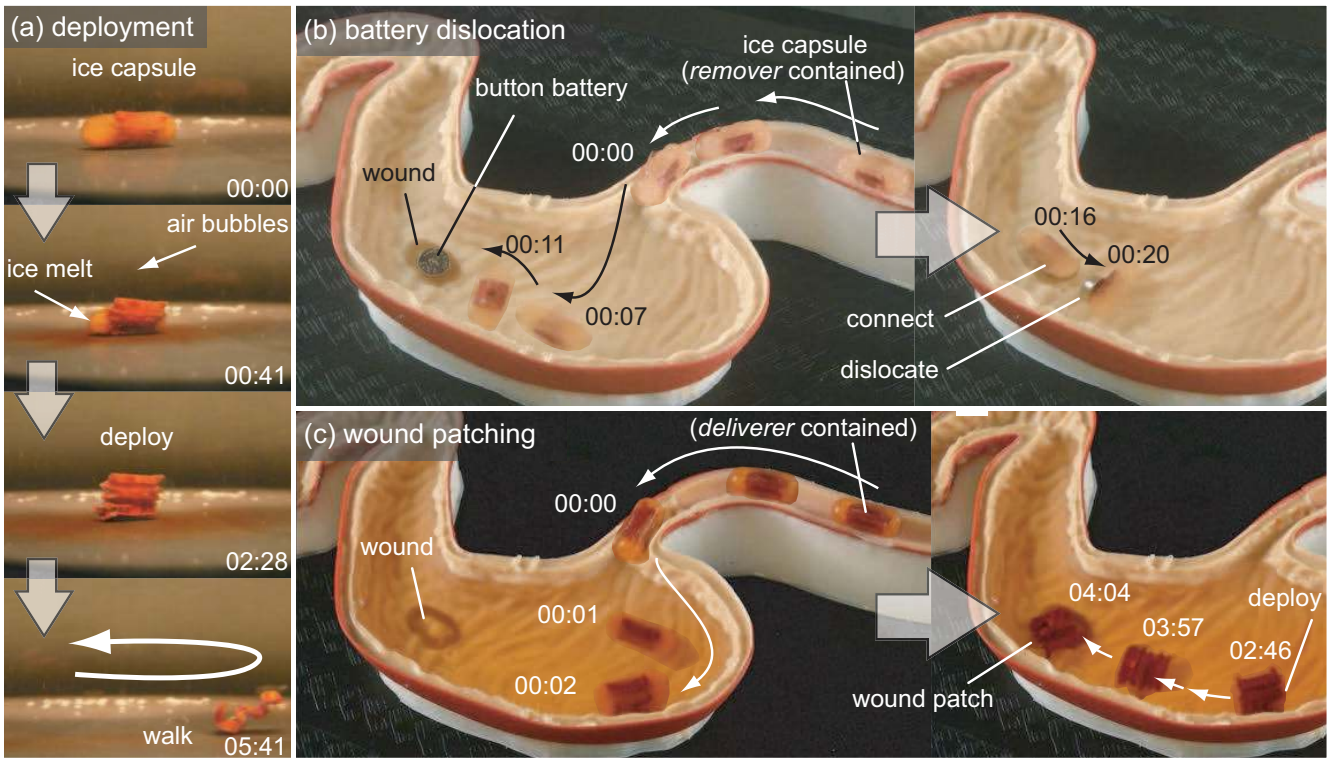

Fig. 8. Task performances. (a) An ice capsule was put into water at room temperature. *Deliverer* deployed in about 3 minutes and was controlled for walking motion. (b) Battery removal experiment. The ice capsule containing *remover* thrown manually into the stomach was controlled remotely and connected to the button battery. The ice capsule successfully dislocated the battery from the site. (c) Wound patching experiment. The thrown ice capsule containing *deliverer* melted in about 3 minutes, transformed into *deliverer*, and subsequently moved onto the wound. For detail, see the supporting video.

V. Experimental Results

In this section we show proof of concept results for robot deployment via capsule melting, removing a button battery, and patching a wound in the artificial stomach.

A. Robot deployment via capsule melting

The dissolution of the ice capsule and the deployed robot's subsequent walking motion are demonstrated in Fig. 8 (a). The *deliverer* was deployed in the stomach as an ice capsule that facilitates the robot transportation by lowering friction with the walls of the esophagus and by preserving the robot's structure and properties. We tested melting the capsule in liquids at a room temperature of 20°C. The dissolution time varies depending on the water temperature. According to our measurements, it took $\sim$ 3 min at 22°C, and $\sim$ 1 min at 28°C (sample number = 5). Water at body temperature should accelerate the speed. Immediately after the ice capsule melted, the robot's body started to be deployed. Once the robot regained the original form, it showed a stable motion underwater under the application of a magnetic field.

B. Ice capsule's roll and foreign body dislocation

The ice capsule dislocating a button battery from the battery-caused inflammation site is shown in Fig. 8 (b). As soon as the ice capsule that contained the *deliverer* was manually transported to the stomach (00:00), the capsule was actuated for rolling motion by an external magnetic field and visually guided to the button battery location. The ice capsule then connected to the battery, and subsequently dislocated the battery (00:16$\sim$00:20). Note that during the operation, the ice melted and continuously reduced the distance between the magnet of the *deliverer* and the battery, assisting torque inductions of different magnitudes and angles. After the ice capsule connected to the battery, they could be discharged out of the body through the gastrointestinal tract.

C. Deliverer's wound patching

We employed the *deliverer* in the artificial stomach for the treatment of the artificially-created ulcer and showed the result in Fig. 8 (c). In this proof of concept experiment, an ice capsule was transported through an esophagus (00:00) and melted in water (23°C) in the stomach; the *deliverer* regained the target body form (02:46), walked (03:57), and patched (floated over the target location) over a simulated ulcer (04:04). Sometimes air bubbles hindered *deliverer* from deployment, and thus we needed to let it tumble for a short duration (between 02:46 and 03:57). We iterated the process 5 times and obtained an average duration of procedure completion of $\sim$ 5 min. The demonstration proves the concept that a biodegradable artificial robot can be dispatched into the artificial stomach to accomplish a mechanical task for a medical purpose.

VI. Discussion & Conclusion

In this paper, we present origami robots that are ingestible and can be controlled to move, manipulate, and accomplish clinically-relevant tasks, such as removing a foreign body and patching a wound in the stomach. Our contributions include the design and fabrication of laminated biodegradable drug-including sheets for the robot's body, a method for ice encapsulation for robot delivery, control, actuation of rolling and locomotion under water, physics models for these motions, and experimental testing in a realistic artificial environment. Our approach requires limited on-board electronics. These minimalist robots enable minimally invasive clinical intervention, and greater flexibility and control in the choice of composite materials to fabricate biocompatible and biodegradable robots that can operate *in vivo*. Additionally, origami capabilities enable reconfigurability for minimal space occupancy and for accomplishing versatile mechanical tasks controlled by an external remote magnetic field.

Our future work includes investigating the safety of our method with respect to long-term biodegradability, and removal and discharge of foreign objects *in vivo*.

Acknowledgment

We thank Kodiak Brush, Alicia Cabrera-Mino, Nikita Waghani, and Kevin A. Gonzales for their support in fabricating the robots and in experiments.

References

[1] S. Miyashita, S. Guitron, M. Ludersdorfer, C. Sung, and D. Rus, "An untethered miniature origami robot that self-folds, walks, swims, and degrades," in *IEEE International Conference on Robotics and Automation (ICRA)*, Seattle, USA, June 2015, pp. 1490–1496.

[2] [Online]. Available: http://poison.org/battery

[3] Z. Nagy, R. Oung, J. J. Abbott, and B. J. Nelson, "Experimental investigation of magnetic self-assembly for swallowable modular robots," in *IEEE/RSJ International Conference on Intelligent Robots and Systems (IROS)*, 2008, pp. 1915–1920.

[4] M. Nokata, S. Kitamura, T. Nakagi, T. Inubushi, and S. Morikawa, "Capsule type medical robot with magnetic drive in abdominal cavity," in *IEEE RAS & EMBS International Conference on Biomedical Robotics and Biomechatronics (BioRob)*, 2008, pp. 348–353.

[5] F. Carpi and C. Pappone, "Magnetic maneuvering of endoscopic capsule by means of a robotic navigation system," *IEEE Transactions on Biomedical Engineering*, vol. 56, no. 5, pp. 1482–1490, 2009.

[6] G.-S. Lien, , C.-W. Liu, J.-A. Jiang, C.-L. Chuang, and M.-T. Teng, "Magnetic control system targeted for capsule endoscopic operations in the stomach - design, fabrication, and in vitro and ex vivo evaluations," *IEEE Transactions on Biomedical Engineering*, vol. 59, no. 7, pp. 2068–2079, 2012.

[7] S. Yim, K. Goyal, and M. Sitti, "Magnetically actuated soft capsule with the multimodal drug relase function," *IEEE/ASME Transactions on Mechatronics*, vol. 18, no. 4, pp. 1413–1418, 2013.

[8] C. Lee, H. Choi, G. Go, S. Jeong, S. Y. Ko, J.-O. Park, and S. Park, "Active locomotive intestinal capsule endoscope (alice) system: A prospective feasibility study," *IEEE/ASME Transactions on Mechatronics*, vol. 20, no. 5, pp. 2067–2074, 2015.

[9] P. Valdastri, M. Simi, and R. J. Webster III, "Advanced technologies for gastrointestinal endoscopy," *Annual Review of Biomedical Engineering*, vol. 14, pp. 397–429, 2012.

[10] M. P. Kummer, J. J. Abbott, B. E. Kratochvil, R. Borer, A. Sengul, and B. J. Nelson, "Octomag: An electromagnetic system for 5-dof wireless micromanipulation," in *IEEE International Conference on Robotics and Automation (ICRA)*, 2010, pp. 1006–1017.

[11] D. D. Damian, S. Arabagi, A. Fabozzo, P. Ngo, R. Jennings, M. Manfredi, and P. E. Dupont, "Robotic implant to apply tissue traction forces in the treatment of esophageal atresia,," in *IEEE International Conference on Robotics and Automation (ICRA)*, 2014, pp. 786–792.

[12] L. Yan, T. Wang, D. Liu, J. Peng, Z. Jiao, and C.-Y. Chen, "Capsule robot for obesity treatment with wireless powering and communication," *IEEE Transactions on Industrial Electronics*, vol. 62, no. 2, pp. 1125–1133, 2015.

[13] K. Kuribayashi, K. Tsuchiya, Z. You, D. Tomus, M. Umemoto, T. Ito, and M. Sasaki, "Self-deployable origami stent grafts as a biomedical application of Ni-rich TiNi shape memory alloy foil," *Materials Science and Engineering A*, vol. 419, pp. 131–137, 2006.

[14] B. J. Nelson, I. K. Kaliakatsos, and J. J. Abbott, "Microrobots for minimally invasive medicine," *Annual Review of Biomedical Engineering*, vol. 12, pp. 55–85, 2010.

[15] S. Hauert and S. N. Bhatia, "Mechanism of cooperation in cancer nanomedicine: towards systems nanotechnology," *Trends in Biotechnology*, vol. 32, pp. 448–455, 2014.

[16] I. D. Falco, G. Tortora, P. Dario, and A. Menciassi, "An integrated system for wireless capsule endoscopy in a liquid-distended stomach," *IEEE Transactions on Biomedical Engineering*, vol. 61, no. 3, pp. 794–804, 2014.

[17] P. Glass, E. Cheung, and M. Sitti, "A legged anchoring mechanism for capsule endoscopes using micropatterned adhesives," *IEEE Transactions on Biomedical Engineering*, vol. 55, no. 12, pp. 2759–2767, 2008.

[18] S. Fusco, H.-W. Huang, K. E. Peyer, C. Peters, M. Haberli, AndreUlbers, A. Spyrogianni, E. Pellicer, J. Sort, S. E. Pratsinis, B. J. Nelson, M. S. Sakar, and S. Pane, "Shape-switching microrobots for medical applications: The influence of shape in drug delivery and locomotion," *ACS Applied Materials and Interfaces*, vol. 7, pp. 6803–6811, 2015.

[19] S. Miyashita, C. D. Onal, and D. Rus, "Self-pop-up cylindrical structure by global heating," in *IEEE/RSJ International Conference on Intelligent Robots and Systems (IROS)*, 2013, pp. 4065–4071.

[20] R. W. Fox, A. T. McDonald, and P. J. Richard, *Fluid Mechanics (8th Edition)*. John Wiley & Sons, Inc., 2011.